

Behavior of concrete-filled double skin steel tube beam-columns

Maha M. Hassan^{*}, Ahmed A. Mahmoud^a and Mohammed H. Serror^b

Structural Engineering Department, Cairo University, Gamaa Street, Giza, Egypt

(Received March 12, 2016, Revised October 28, 2016, Accepted November 12, 2016)

Abstract. Concrete-filled double skin steel tube (CFDST) beam-columns are widely used in industrial plants, subways, high-rise buildings and arch bridges. The CFDST columns have the same advantages as traditional CFT members. Moreover, they have lighter weight, higher bending stiffness, better cyclic performance, and have higher fire resistance capacities than their CFT counterparts. The scope of this study is to develop finite element models that can predict accepted capacities of double skin concrete-filled tube columns under the combined effect of axial and bending actions. The analysis results were studied to determine the distribution of stresses among the different components and the effect of the concrete core on the outer and inner steel tube. The developed models are first verified against the available experimental data. Accordingly, an extensive parametric study was performed considering different key factors including load eccentricity, slenderness ratio, concrete compressive strength, and steel tube yield strength. The results of the performed parametric study are intended to supplement the experimental research and examine the accuracy of the available design formulas.

Keywords: beam-columns; concrete-filled tube; double-skin; parametric study

1. Introduction

Composite systems that combine steel and concrete in a global structural system are an effective and economical solution to resist different expected straining actions. The structural combination of steel and concrete gives many benefits in terms of strength, mass, damping properties, cost, speed of construction, and fire protection. Consequently, composite systems have become a popular system in different constructions such as high-rise buildings, bridges, piers, and lateral loads resisting systems. In most composite systems, composite columns are used to resist vertical and lateral loads. Since the basic function of the column is to carry vertical forces, it is important to reach the required design strength and serviceability limit state with the least usage of area; this can be achieved by efficient and economical arrangement of steel and concrete in the cross section. Concrete-filled double skin steel tube (CFDST) beam-columns represent an efficient and economic structural system that combines the benefits of steel and concrete in a more efficient manner compared to traditional concrete-filled tube (CFT) ones. CFDST beam-columns consist of an outer and inner steel encasement filled with poured concrete between them; the steel outer and inner encasement could be pipe, tube, or any hollow section with different possible configurations

^{*}Corresponding author, Assistant Professor, E-mail: mahamoddather@eng.cu.edu.eg

^aM.Sc. Student, E-mail: eng.ashraf27@yahoo.com

^bAssociate Professor, E-mail: mhassanien@cosmos-eng.com

as shown in Fig. 1.

Although CFDST elements are often considered as new type of construction, its development has been the subject of extensive research over the past decades. The axial or flexural behavior of them was examined by different researchers. It was generally observed that the strength of CFDST elements is higher than the summation of the strength of their individual elements. Due to their great advantages, there has been increasing demand for using CFDST in offshore construction, highways and high-rise bridge piers. It is also expected that CFDST columns have a considerable potential to be used in building structures. The available literature shows different research efforts investigating the behavior of CFDST beam-columns and suggesting design formulas for their capacities. The studied parameters included inner-to-outer diameter ratio, diameter-to-thickness ratio, hollow section ratio and the magnitude of the axial load.

Lin and Tsai (2001) tested nine CFDST beam-columns. The results showed the efficient behavior of such elements even with large diameter-to-thickness ratios. Tao *et al.* (2004) developed a theoretical model for CFDST stub columns and beam-columns based on the results of a series of tests on CFDST having circular inner and outer tubes. Han *et al.* (2004) performed a series of tests on CFDST stub columns, beams, and beam-columns having square hollow section for the outer tube and circular hollow section for the inner tube. Hence, simplified interaction curves were derived for CFDST beam-columns. Huang *et al.* (2010) performed an extensive parametric study based on previous experimental programs and provided insight over the effect of different parameters. Tao and Han (2006) carried out a series of tests, including three stub columns, three beams and twenty-four beam-columns. Accordingly, the load-deformation behavior was compared to conventional concrete-filled steel tubular members and empty double skin tubular members. Moreover, theoretical models for CFDST stub columns, beams and beam-columns with rectangular inner and outer steel tubes were established. Uenaka *et al.* (Uenaka *et al.* 2008a, b, 2010, Uenaka and Kitoh 2009) investigated the axial and bending characteristics of CFDST experimentally while focusing on two test parameters: inner-to-outer diameter ratio and thickness-to-diameter ratio. Uenaka and Kitoh (2011) investigated the mechanical behavior of CFDST deep beam under a combined action of shear and bending through three-point static loading test. Focus was also given to the effect of the inner-to-outer diameter ratio (D_i/D_o) and the outer tube diameter-to-thickness ratio (D_o/t_o). In addition to the above research efforts, the cyclic behavior of CFDST beam-columns was extensively investigated through experimental and analytical studies (Han *et al.* 2006, 2009a, Yagishita *et al.* 2000). The effect of long-term loadings on the performance of CFDST columns was experimentally investigated by Han *et al.* (2009b). The characteristics of behavior after exposure to fire was investigated mainly for axially loaded columns (Yu *et al.* 2009, Lu *et al.* 2011). Han *et al.* (2014) explored the developments in the use of CFDST sections and the available design formulas suggested by codes and researchers. Pagoulatou *et al.* (2014) offered a formula for predicting the member capacity of CFDST columns based on modifications of the approach adopted by Eurocode 4 (EC4) for concrete-filled steel tubes. The study focused on members subjected to concentric axial load through an extensive parametric study. Ho and Dong (2014) investigated the effect of using external ring stiffeners in order to increase the confining performance of steel tubes in the early elastic stage of axial loading through experimental testing of twenty units. The authors suggested a simplified design formula for confined axially loaded CFDST sections. Ren *et al.* (2014) investigated the behavior of tapered CFDST stub columns subjected to axial partial compression while considering tapering angle, top endplate thickness, and partial compression area ratio. Accordingly, a formula was proposed to predict the cross-sectional capacity of the tapered CFDST sections under axial partial compression.

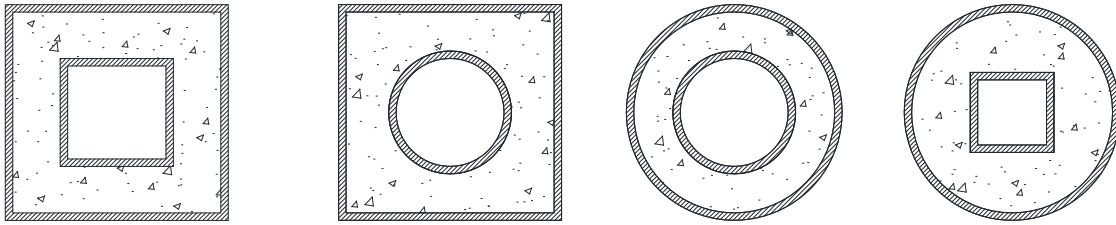


Fig. 1 Different configuration of concrete-filled double skin steel tubes

The current study aims to examine the overall behavior of CFDST beam-columns having circular inner and outer steel tubes tested under the effect of eccentric axial compressive forces. Finite element models are built using ANSYS software program. Models are verified by comparison to the test results reported by Tao *et al.* (2004). An extensive parametric study is conducted to investigate the effect of load eccentricity, slenderness ratio, different geometric parameters, and material strength properties on combined axial and flexural nominal strength of CFDST. Accordingly, the parametric study results are compared to the theoretical and simplified models available in literature. The study focuses on the practical aspects followed by regular designers who will not resort to advanced time-consuming finite element models. Hence, in the current study, capacity formulas listed in AISC-360-10 (2010) for concrete-filled sections are extended to account for the internal steel tube. Accordingly, capacity predictions are calculated and tested against the parametric study results

2. Numerical analysis method

2.1 Analysis procedure

Three-dimensional models representing CFDST beam-columns are built using ANSYS 12 finite element software. The models simulated the different components of the CFDST beam-columns including the inner steel tube, the concrete core, and the outer steel tube. Selection of elements and meshing size is decided based on a sensitivity analysis in order to obtain accurate results with reasonable computing time. The inner and outer steel tubes are modeled using eight-node 3D (SOLID45) elements (Huang *et al.* 2010). The concrete core is modeled using concrete (SOLID65) elements. Fig. 2 shows the modeling of the different parts comprising the model. Fig. 3 shows a general view of the finite element model including the mesh structure.

2.2 Material constitutive relationship

The simulated models in the verification step and the parametric study include steel and concrete components. An elastic plastic stress-strain relation model consisting of five stages (i.e., elastic, elastic-plastic, plastic, hardening and fracture) is used. A bilinear stress-strain curve for steel is assumed, Fig. 4 (Pagoulatou *et al.* 2014). The steel is assumed to have isotropic hardening behavior, i.e., the yield surface changes uniformly in all directions so that yield stresses increase or decrease in all stress directions when plastic straining occurs. Elastic modulus (E_s) and Poisson's ratio, ν_s , for steel are taken as 2×10^5 N/mm² and 0.3, respectively.

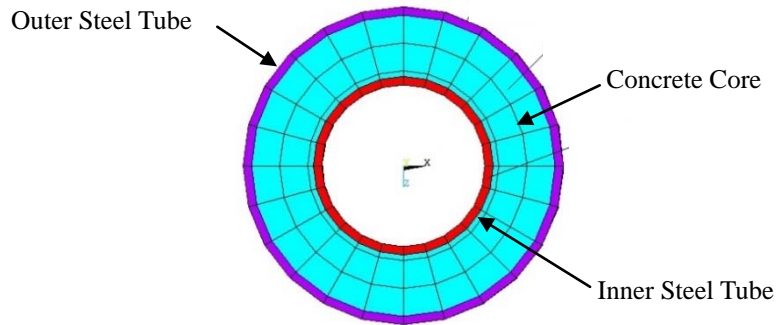


Fig. 2 Main Components of Models

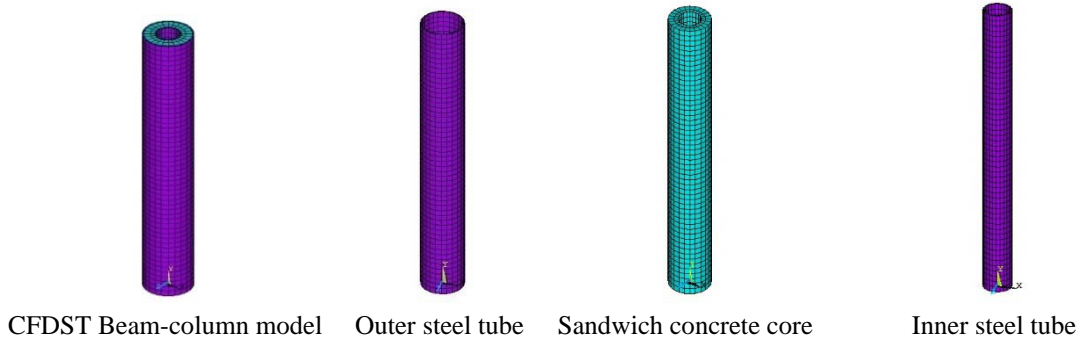


Fig. 3 General view of the finite element model

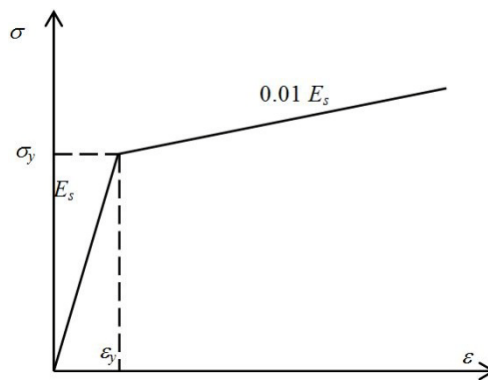


Fig. 4 Stress-strain curve of steel

The material constitutive relation for concrete is automatically computed by the program after defining Poisson’s ratio, Young’s modulus, open shear transfer coefficient, closed shear transfer coefficient, uniaxial cracking stress, and uniaxial crushing stress. Other material parameters were automatically set to the program default values. Concrete is a brittle material with different failure mechanism in compression and tension, i.e., crushing in compression and cracking in tension.

Hence, uniaxial cracking stress of concrete is taken as 10% of its compressive strength. Open shear transfer coefficient is set equal to 0.3, whereas closed shear transfer coefficient is set equal to 0.9. The initial modulus of elasticity, E_c , and Poisson's ratio, ν_c , of concrete are determined according to the recommendations in ACI 318-14 (2014), given as $E_c = 4700\sqrt{f_{ck}}$ and $\nu_c = 0.2$, respectively. The confinement effect is considered through the confinement coefficient (ξ) (Huang *et al.* 2010).

2.3 Loads and boundary conditions

Fig. 5 shows the applied boundary conditions on the model. For the top end of the model, the top area of the steel plate was constrained in X and Z direction to represent hinged support at the top end of the beam-column. For the bottom end of the model, only the node in the eccentricity distance (in X -direction) was constrained in all direction to represent hinged support at the bottom end of the beam-column. By this way, the beam-column will be able to act as a pin-ended support. The eccentric load was applied on one node located at the eccentricity distance.

The load is applied as a concentrated load with eccentricity (e) to a node located at the upper surface of the rigid plate at the top of the model. The load is applied incrementally by dividing it into a series of load steps and the analysis is terminated when the limit load or the nominal load of CFDST is reached.

2.4 Nonlinear solution and convergence criteria

At the completion of each incremental solution, the stiffness matrix of the model is adjusted to reflect nonlinear changes in structural stiffness proceeding to the next load increment. The ANSYS software program uses Newton-Raphson equilibrium iterations for updating the model stiffness. Newton-Raphson equilibrium iterations provide convergence at the end of each load increment within the specified tolerance limits. In this study, force convergence criterion is chosen and the convergence tolerance limits are adjusted to 5%. Sources of nonlinearity in the model are essentially caused by the material models.

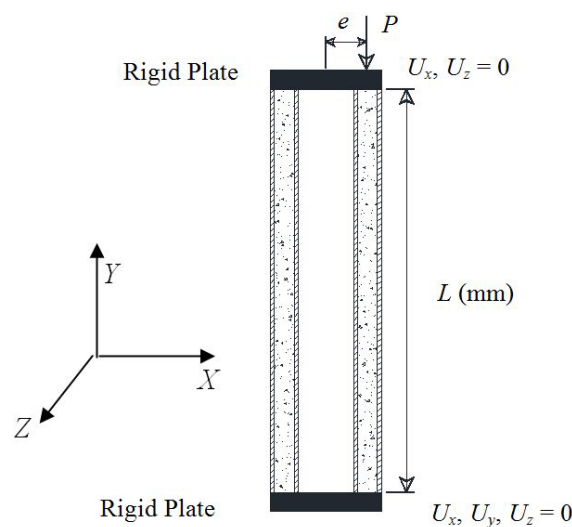


Fig. 5 Considered boundary conditions on model

2.5 Verification against experimental results

The simplified nonlinear fiber element method is verified by comparing the results from this method to experimental results carried out by Tao *et al.* (2004). The purpose of the verification is to prove that the proposed finite model can provide reasonable results for parametric study analysis. Table 1 lists the geometrical and material properties of different specimens. All twelve tested specimens were composed of inner and outer circular steel tubes filled in between with concrete and having a 30 mm steel plate in the top and bottom end. The specimens were eccentrically loaded until failure. Each two successive specimens have the same geometrical and material properties. The compressive strength of concrete cubes (f_{cu}) at the time of testing was 46.3 N/mm². The modulus of elasticity (E_c) of concrete was found equal to 33,300 N/mm². Steel yield stress for outer tubes (f_{syo}) and inner tubes (f_{syi}) were 294.5 and 374.5 N/mm², respectively. Same value was used for the diameter of the outer steel tube, D_o , the thickness of the outer steel tube, t_{so} , the diameter of the inner steel tube, D_i , and the thickness of the inner steel tube, t_{si} . The studied variables included the load eccentricity, e , the slenderness ratio, λ , and the hollow section ratio of the composite section, χ .

2.5.1 Failure mode

Typical failure mode of beam-columns is overall buckling failure. Fig. 6 gives a general view of the specimens at the end of loading compared to the finite element model at the maximum attained load. When the load was small, the lateral deflection of the specimen at middle height was small and approximately proportional to the applied load. As the load reached about 60-70% of the maximum load, the lateral deflection at middle height started to increase significantly.

2.5.2 Comparison of results

The results of the numerical simulation are compared to the experimental equivalent ones. Table 2 shows The ultimate load of CFDST beam-column obtained from finite element modeling,

Table 1 Geometry and mechanical properties of verification models

No.	Specimen Label	$D_o \times t_{so}$ (mm)	$D_i \times t_{si}$ (mm)	D_o/t_{so}	χ	L (mm)	λ	f_{syo} (N/mm ²)	f_{syi} (N/mm ²)	e (mm)
1	Pcc1-1a	114×3	58×3	38	0.54	887	28	294.5	374.5	4
2	Pcc1-1b	114×3	58×3	38	0.54	887	28	294.5	374.5	4
3	Pcc1-2a	114×3	58×3	38	0.54	887	28	294.5	374.5	14
4	Pcc1-2b	114×3	58×3	38	0.54	887	28	294.5	374.5	14
5	Pcc1-3a	114×3	58×3	38	0.54	887	28	294.5	374.5	45
6	Pcc1-3b	114×3	58×3	38	0.54	887	28	294.5	374.5	45
7	Pcc2-1a	114×3	58×3	38	0.54	1770	56	294.5	374.5	0
8	Pcc2-1b	114×3	58×3	38	0.54	1770	56	294.5	374.5	0
9	Pcc2-2a	114×3	58×3	38	0.54	1770	56	294.5	374.5	15.5
10	Pcc2-2b	114×3	58×3	38	0.54	1770	56	294.5	374.5	15.5
11	Pcc2-3a	114×3	58×3	38	0.54	1770	56	294.5	374.5	45
12	Pcc2-3b	114×3	58×3	38	0.54	1770	56	294.5	374.5	45



Fig. 6 General view of the failure mode of verification model vs. Tested specimen

NFE, the ultimate load of CFDST beam-column resulted from experimental tests, $N_{Exp.}$, and mid-height deflection, Δ . The ratio between the experimental and simulation results is also exhibited. Figs. 7 and 8 summarize the comparison of the finite element and the experimental study results. The average error of the axial capacity is 2.4% and the maximum error is 5.7%. This small error indicates that the proposed modeling technique is capable to estimate the nominal strength of CFDST beam-column. As for the mid-height displacement, the average error reached 15.6%. It is observed that for the units with small eccentricity ratio the value of the relative error for mid-height displacement increases. For these models, the ultimate load is reached; however, any increase in the load failed to attain a convergent solution. This is attributed for using a force control criteria in the analysis. The attained accuracy is considered sufficient for the current study as the ultimate capacity of sections is the value derived from the models.

Table 2 Axial load capacities and corresponding mid-height displacements for verification models

No.	Specimen label	Ultimate load (kN)		$\frac{N_{FE}}{N_{Exp.}}$	Δ (mm)		$\frac{\Delta_{FE}}{\Delta_{Exp.}}$
		$N_{Exp.}$	N_{FE}	$N_{Exp.}$	$\Delta_{Exp.}$	Δ_{FE}	$\Delta_{Exp.}$
1	Pcc1-1a	664	650	0.98	1.4	0.9	0.64
2	Pcc1-1b	638	650	1.02	1.1	0.9	0.82
3	Pcc1-2a	536	550	1.03	3.0	3	1.00
4	Pcc1-2b	549	550	1.00	3.0	3	1.00
5	Pcc1-3a	312	320	1.03	5.3	5.1	0.96
6	Pcc1-3b	312	320	1.03	5.2	5.1	0.98
7	Pcc2-1a	620	600	0.97	0.3	0.2	0.67
8	Pcc2-1b	595	600	1.01	0.3	0.2	0.67
9	Pcc2-2a	400	400	1.00	7.0	7.2	1.03
10	Pcc2-2b	394	400	1.02	6.5	7.2	1.11
11	Pcc2-3a	228	240	1.05	14.0	13	0.93
12	Pcc2-3b	227	240	1.06	14.0	13	0.93

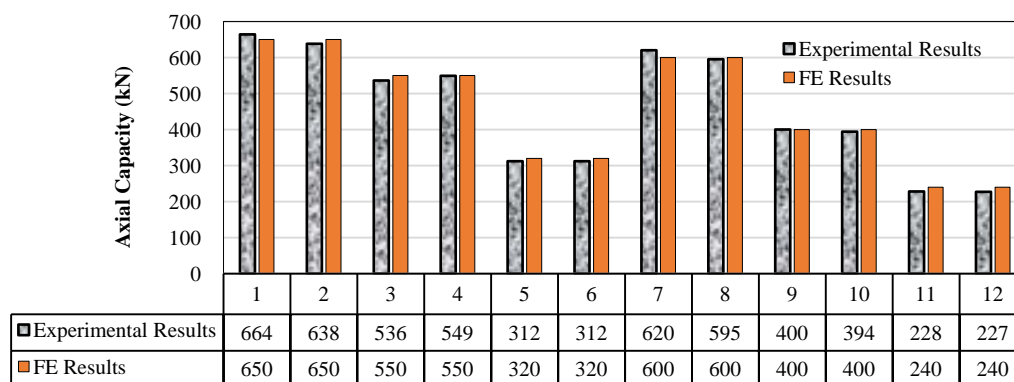


Fig. 7 Comparison between Experimental and FE Axial Load Capacities for Verification Models

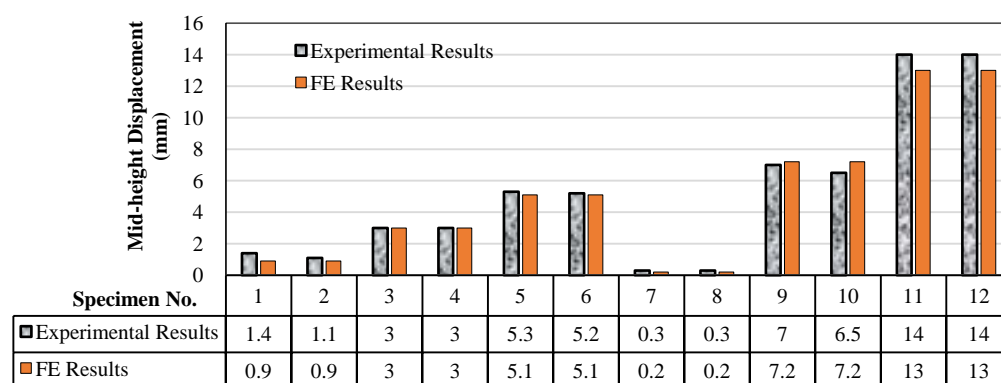


Fig. 8 Comparison between Experimental and FE Mid-height Displacement for Verification Models

Figs. 9(a) and 9(b) exhibit the axial load versus mid-height deflection for verification models 5 and 6; and 9 and 10. As can be seen, the numerical results show good agreement with the experimental data. Based on the above comparisons, the model results are found to be reliable and can be used to simulate CFDST beam-column with extended parameters and loading conditions.

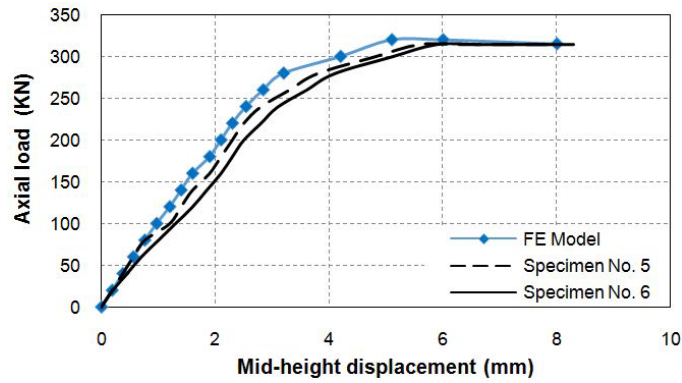
2.6 Parametric analysis

A total of fifty-four models are prepared to investigate the influences of various parameters on the combined axial and flexural capacity of circular CFDST beam-columns. The outer and inner diameters of the steel tubes are unified for all models as 114 and 57 mm, respectively; and the steel tube thickness is considered equal to 3 mm. The used studied parameters are as follows:

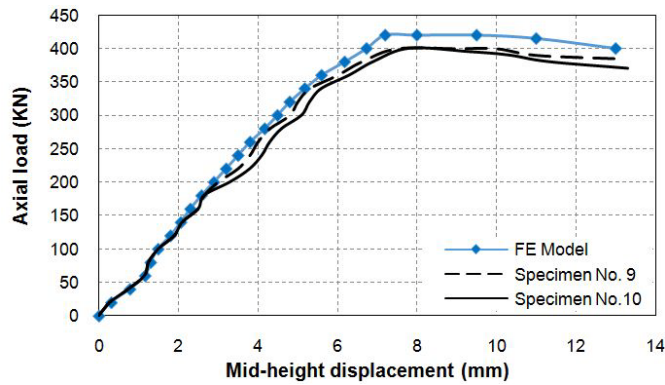
- Load eccentricity ($e\%$): 0, 50, and 100 %.
- Slenderness ratio (λ): 25, 50, and 80.
- Compressive strength of concrete cube after 28 days, f_{cu} (N/mm^2): 30, 50, and 90.
- Yield strength of steel tube, f_y (N/mm^2): 235, and 360.

The parameters are interchanged between the different models in order to study the influence of

each independent variable separately; whereas other independent parameters were kept unchanged. Table 3 summarizes the characteristics of the models adopted and modeled in the current study.



(a) Specimens No. 5 and 6



(b) Specimens No. 9 and 10

Fig. 9 Axial load (N) versus Mid-height lateral deflection (Δ) curves for different verification models

Table 3 Dimensions and material properties of parametric study CFDST models

Model No.	Dimensions				Material properties			Steel ratio (χ)	$e\%$	λ
	D_o (mm)	t_o (mm)	D_i (mm)	t_i (mm)	L (mm)	f_y (N/mm ²)	f_{cu} (N/mm ²)			
1	114	3	57	3	792	235	30	0.54	0	25
2	114	3	57	3	792	235	30	0.54	50	25
3	114	3	57	3	792	235	30	0.54	100	25
4	114	3	57	3	792	235	50	0.54	0	25
5	114	3	57	3	792	235	50	0.54	50	25
6	114	3	57	3	792	235	50	0.54	100	25
7	114	3	57	3	792	235	90	0.54	0	25
8	114	3	57	3	792	235	90	0.54	50	25

Table 3 Continued

Model No.	Dimensions					Material properties		Steel ratio (χ)	$e\%$	λ
	D_o (mm)	t_o (mm)	D_i (mm)	t_i (mm)	L (mm)	f_y (N/mm ²)	f_{cu} (N/mm ²)			
9	114	3	57	3	792	235	90	0.54	100	25
10	114	3	57	3	1584	235	30	0.54	0	50
11	114	3	57	3	1584	235	30	0.54	50	50
12	114	3	57	3	1584	235	30	0.54	100	50
13	114	3	57	3	1584	235	50	0.54	0	50
14	114	3	57	3	1584	235	50	0.54	50	50
15	114	3	57	3	1584	235	50	0.54	100	50
16	114	3	57	3	1584	235	90	0.54	0	50
17	114	3	57	3	1584	235	90	0.54	50	50
18	114	3	57	3	1584	235	90	0.54	100	50
19	114	3	57	3	2534	235	30	0.54	0	80
20	114	3	57	3	2534	235	30	0.54	50	80
21	114	3	57	3	2534	235	30	0.54	100	80
22	114	3	57	3	2534	235	50	0.54	0	80
23	114	3	57	3	2534	235	50	0.54	50	80
24	114	3	57	3	2534	235	50	0.54	100	80
25	114	3	57	3	2534	235	90	0.54	0	80
26	114	3	57	3	2534	235	90	0.54	50	80
27	114	3	57	3	2534	235	90	0.54	100	80
28	114	3	57	3	792	360	30	0.54	0	25
29	114	3	57	3	792	360	30	0.54	50	25
30	114	3	57	3	792	360	30	0.54	100	25
31	114	3	57	3	792	360	50	0.54	0	25
32	114	3	57	3	792	360	50	0.54	50	25
33	114	3	57	3	792	360	50	0.54	100	25
34	114	3	57	3	792	360	90	0.54	0	25
35	114	3	57	3	792	360	90	0.54	50	25
36	114	3	57	3	792	360	90	0.54	100	25
37	114	3	57	3	1584	360	30	0.54	0	50
38	114	3	57	3	1584	360	30	0.54	50	50
39	114	3	57	3	1584	360	30	0.54	100	50
40	114	3	57	3	1584	360	50	0.54	0	50
41	114	3	57	3	1584	360	50	0.54	50	50
42	114	3	57	3	1584	360	50	0.54	100	50
43	114	3	57	3	1584	360	90	0.54	0	50
44	114	3	57	3	1584	360	90	0.54	50	50
45	114	3	57	3	1584	360	90	0.54	100	50

Table 3 Continued

Model No.	Dimensions					Material properties		Steel ratio (χ)	$e\%$	λ
	D_o (mm)	t_o (mm)	D_i (mm)	t_i (mm)	L (mm)	f_y (N/mm ²)	f_{cu} (N/mm ²)			
46	114	3	57	3	2534	360	30	0.54	0	80
47	114	3	57	3	2534	360	30	0.54	50	80
48	114	3	57	3	2534	360	30	0.54	100	80
49	114	3	57	3	2534	360	50	0.54	0	80
50	114	3	57	3	2534	360	50	0.54	50	80
51	114	3	57	3	2534	360	50	0.54	100	80
52	114	3	57	3	2534	360	90	0.54	0	80
53	114	3	57	3	2534	360	90	0.54	50	80
54	114	3	57	3	2534	360	90	0.54	100	80

3. Results and analysis

The different parametric study models are analyzed and results are deduced from ANSYS software program. Focus is given to the axial capacity, N_{FE} , and flexural capacity, M_{FE} . The sectional combined axial and flexural capacities derived from the models are compared to the sectional axial and flexural ultimate capacities of the section (N_u , M_u) calculated as follows (Tao *et al.* 2004)

$$N_u = N_{osc,u} + N_{i,u} \quad (1)$$

$$M_u = \gamma_m \cdot W_{scm} \cdot f_{scy} + M_{i,u} \quad (2)$$

Where:

- $N_{osc,u}$: The capacity of the outer steel tube with the sandwiched concrete.
- $N_{i,u}$: The compressive capacity of the inner tube.

In the following sections, results of the parametric analysis are presented for each studied independent variable. As can be seen, the attained axial section capacity decreases as the eccentricity increase by an average value of 57% and 70% for eccentricity of 50% and 100% of the section outer diameter, respectively. In addition, the attained axial section capacity decreases as the slenderness ratio increases.

3.1 Influence of load eccentricity (e)

The load eccentricity ($e\%$) on the CFDST beam-column is varied from 0 to 100% of the section outer radius. Figs. 10 through 12 show the effect of increasing the load eccentricity on compressive axial capacity, N_{FE} , and flexural capacity, M_{FE} . The figures also show the increase in the overall capacity of section as the steel yield strength increases. For models having compressive concrete strength equal to 30 MPa, the value of N_{FE} decreased by 38% and 25% as the load eccentricity increased from 0 to 100% for steel yield strength equal to 235 MPa and 360 MPa,

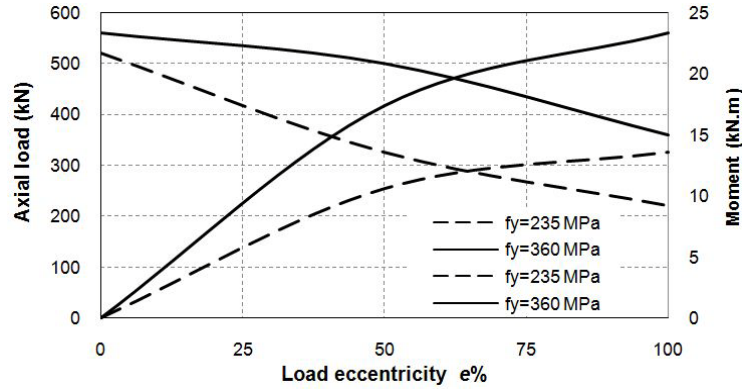


Fig. 10 Axial and flexural capacity (N_{FE} , M_{FE}) versus percentage of eccentricity ($e\%$) for concrete compressive strength = 30 MPa and slenderness ratio = 25

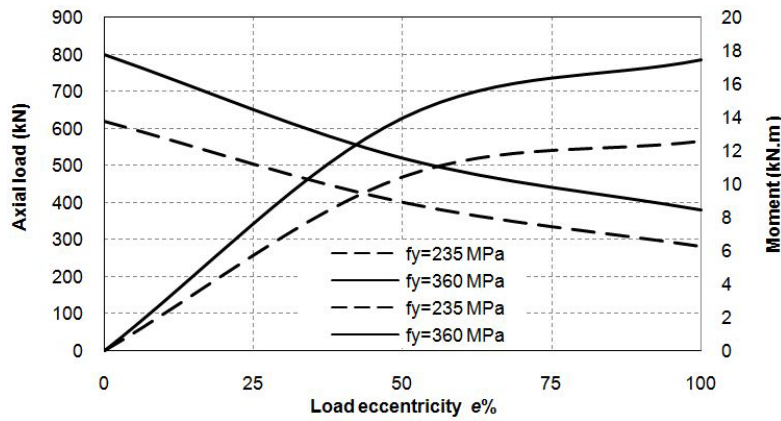


Fig. 11 Axial and flexural capacity (N_{FE} , M_{FE}) versus percentage of eccentricity ($e\%$) for concrete compressive strength = 50 MPa and slenderness ratio = 25

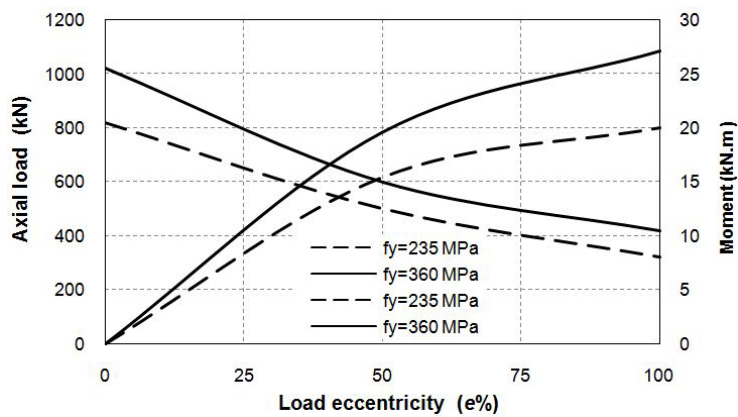


Fig. 12 Axial and flexural capacity (N_{FE} , M_{FE}) versus percentage of eccentricity ($e\%$) for concrete compressive strength = 90 MPa and slenderness ratio = 25

respectively. As the concrete compressive strength increased to 50 MPa, the percentage of decrease of NFE are observed as 48% and 46% as the load eccentricity increased from 0 to 100% for steel yield strength equal to 235 MPa and 360 MPa, respectively. For concrete compressive strength equal to 90 MPa, these ratios reached 52% and 51%. The maximum reduction in axial compressive strength is found to be equal to 82% for model number 54 having $f_y = 360$ Mpa and slenderness ratio = 80.

3.2 Influence of slenderness ratio (λ)

The effect of the slenderness ratio on the CFDST beam-column capacity was investigated. The value of (λ) was varied from 25 to 80, as listed in Table 3. Figs. 13 and 14 show the effect of increasing the slenderness ratio on the compressive axial capacity, NFE, and the flexural capacity, MFE. The effect of slenderness ratio (λ) on the axial compressive strength, NFE, is more pronounced for beam-columns having concrete compressive strength, f_{cu} , steel yield strength, f_y ,

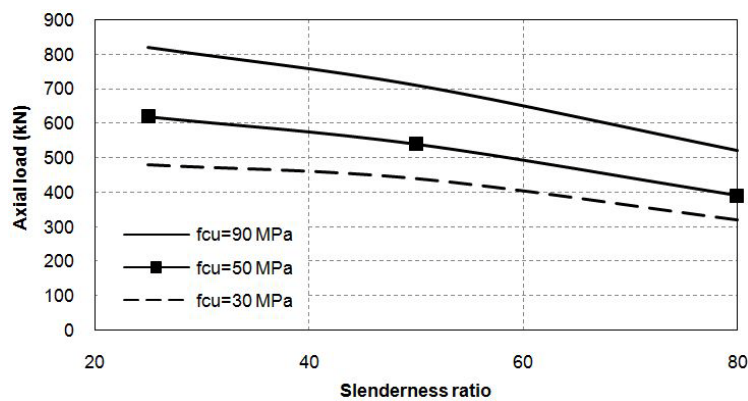


Fig. 13 Axial capacity (N_{FE}) versus slenderness ratio (λ) for steel yield strength = 235 MPa and eccentricity = 0%

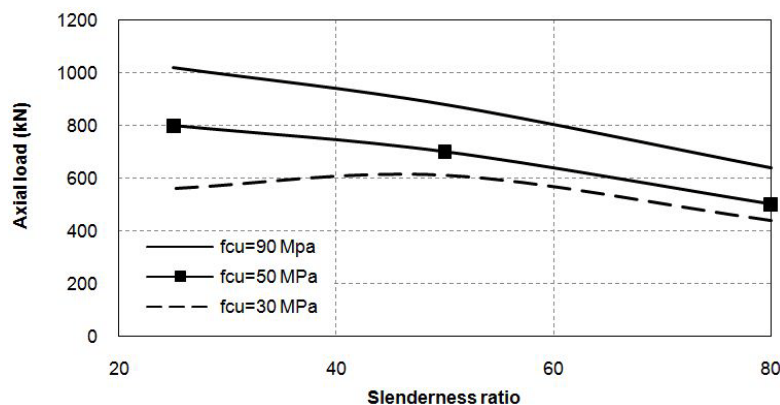


Fig. 14 Axial capacity (N_{FE}) versus slenderness ratio (λ) for steel yield strength = 360 MPa and eccentricity = 0%

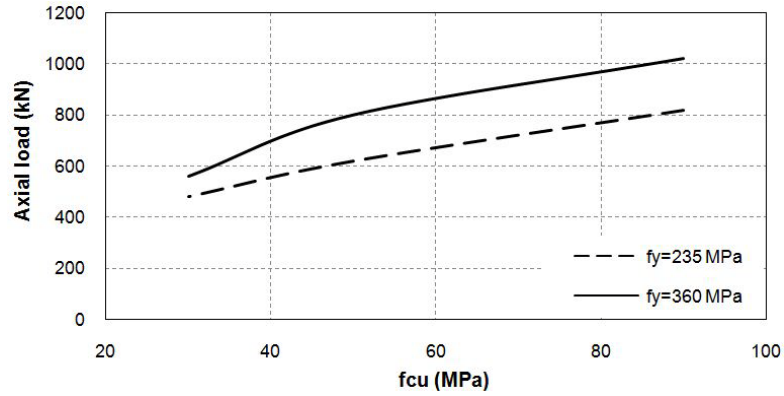


Fig. 15 Axial capacity (N_{FE}) versus concrete compressive strength (f_{cu}) for percentage of load eccentricity = 0% and slenderness ratio = 25

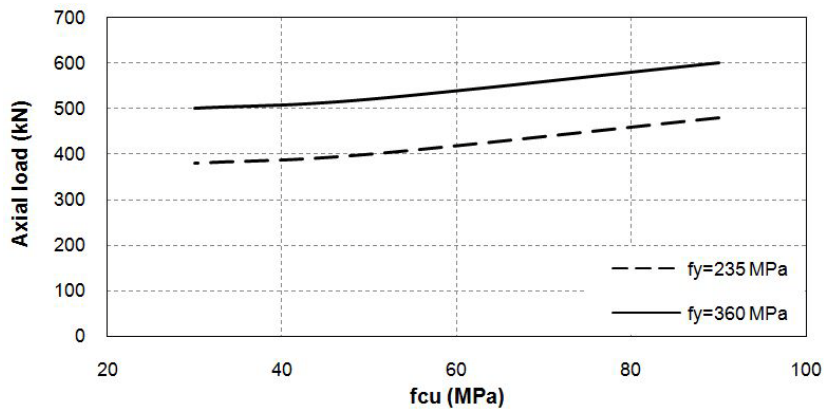


Fig. 16 Axial capacity (N_{FE}) versus concrete compressive strength (f_{cu}) for percentage of load eccentricity = 50% and slenderness ratio = 25

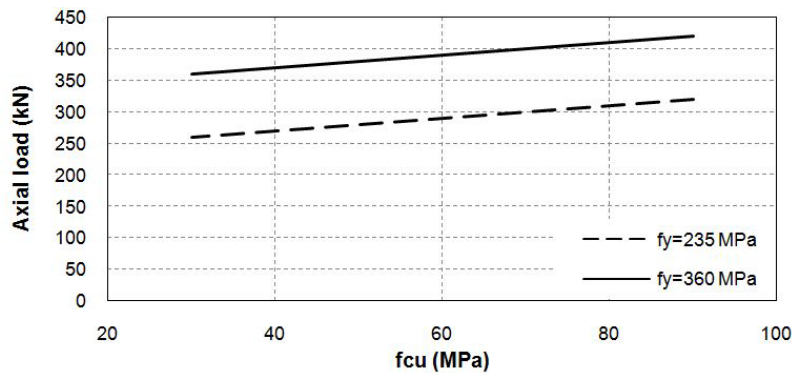


Fig. 17 Axial capacity (N_{FE}) versus concrete compressive strength (f_{cu}) for percentage of load eccentricity = 100% and slenderness ratio = 25

and percentage of load eccentricity, $e\%$, equal to 30 MPa, 235 MPa, and 50%, respectively. For this model, the value of NFE is reduced by 53% as the slenderness ratio increases from 25 to 80. On the other hand, the least reduction in the axial compressive strength, NFE, is noticed in beam-columns having concrete compressive strength, f_{cu} , steel yield strength, f_y , and percentage of load eccentricity, $e\%$, equal to 30 MPa, 360 MPa, and 0%, respectively. For this model, the value of NFE is reduced by 21% as the slenderness ratio increases from 25 to 80. Generally, the relationship between the axial capacity and the slenderness ratio is linear for the different considered material strengths.

3.3 Influence of material strength

Figs. 15 through 17 show the variation in axial load capacity, N_{FE} as the compressive strength of concrete, f_{cu} , and the yield strength of steel, f_y , changes for each load eccentricity and slenderness ratio considered in the parametric analysis. The axial capacity and flexural capacity of the section increase as the compressive strength of concrete, f_{cu} , and the yield strength of steel, f_y , increase. The highest enhancement in the axial capacity of the section as the yield strength of steel increased from 235 MPa to 360 MPa is observed for models number 10 and 37. For these models, the percentage of increase reached 38.6%. Generally, as the slenderness ratio and load eccentricity increases, increasing the steel strength has a more pronounced effect as can be observed from figures.

3.4 Distribution of stresses in CFDST components

Table 4 illustrates the variation in the percentage of compressive and tensile stresses carried by the steel components of the CFDST section along with the variation of the studied independent parameters: slenderness ratio, load eccentricity, concrete compressive strength, and steel yield strength. Increasing the percentage of load eccentricity resulted in imposing the highest tensile stresses on the different components of the section due to the applied axial compressive loading.

Table 4 Influence of independent variables on stress distribution of different components of CFDST

Model No.	Inner steel tube		Outer steel tube		Concrete core		Studied parameter
	Compression %	Tension %	Compression %	Tension %	Compression %	Tension %	
40	46.11%	0.00%	46.31%	0.00%	7.58%	0.00%	$e = 0\%$
41	43.95%	4.16%	47.93%	95.45%	9.10%	0.39%	$e = 50\%$
42	40.63%	23.89%	49.36%	75.95%	10.01%	0.16%	$e = 100\%$
32	44.40%	0.00%	41.01%	98.79%	14.59%	1.21%	$\lambda = 25$
41	43.95%	4.16%	47.93%	95.45%	9.10%	0.39%	$\lambda = 50$
50	26.77%	9.75%	62.63%	88.62%	10.59%	1.64%	$\lambda = 80$
38	33.69%	5.65%	59.63%	94.01%	6.68%	0.34%	$f_{cu} = 30 \text{ MPa}$
41	43.95%	4.16%	47.93%	95.45%	9.10%	0.39%	$f_{cu} = 50 \text{ MPa}$
44	42.27%	9.91%	45.53%	89.53%	12.21%	0.55%	$f_{cu} = 90 \text{ MPa}$
14	44.70%	0.55%	45.85%	98.44%	9.45%	1.01%	$f_y = 235 \text{ MPa}$
41	43.95%	4.16%	47.93%	95.45%	9.10%	0.39%	$f_y = 360 \text{ MPa}$

Fig. 18 shows the stress distribution for the outer steel tube along the length of model number 11. As can be seen, the tensile stresses increase near the middle of the beam-column. Figs. 19(a) through 19(h) show the stress distribution for the inner and the outer steel tube. Increasing the percentage of load eccentricity (models 40, 41, and 42) led to the formation of tensile stresses at the outer most fibers of the outer steel tubes. The ratio of the section subjected to tensile stresses increased as the eccentricity percentage increased. The same behavior is observed as the slenderness ratio increased for models 32, 41, and 50. Increasing the compressive strength of concrete has a minor effect on the stress distribution over the outer steel tube; however, the compressive stresses carried by the inner steel tube increased considerably. Meanwhile, using steel tubes with higher strength increased the stresses carried by the different components of the section by approximately the same ratio.

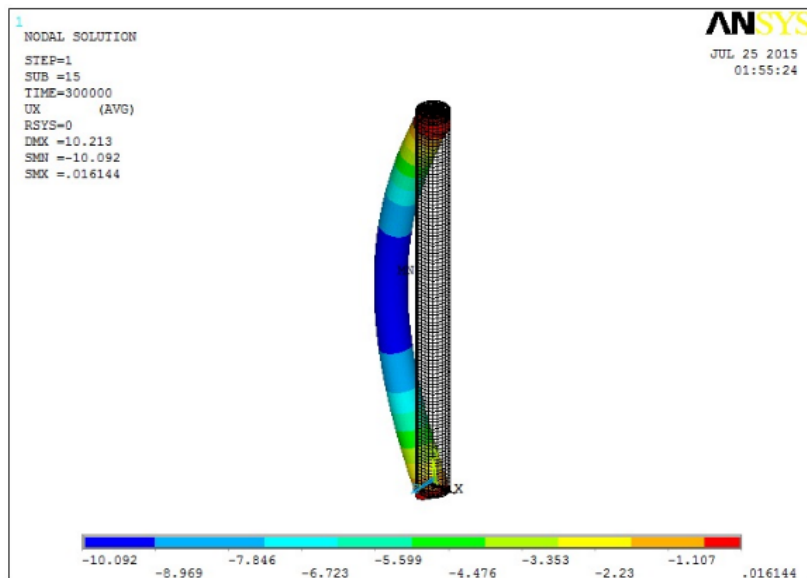
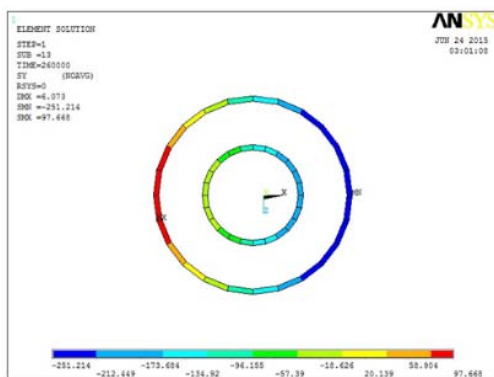
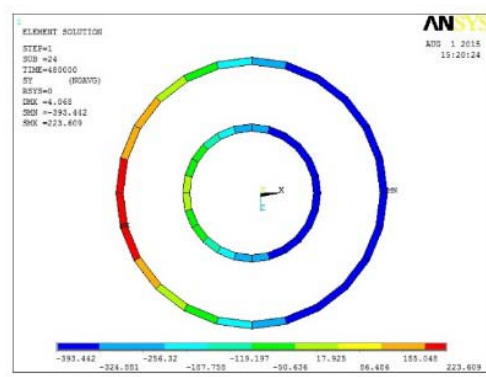


Fig. 18 Stress distribution for the outer steel tube across member length

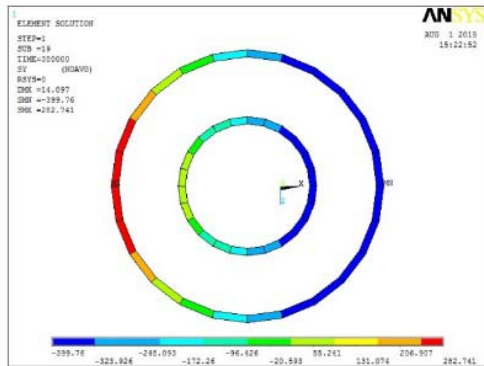


(a) Model No.14

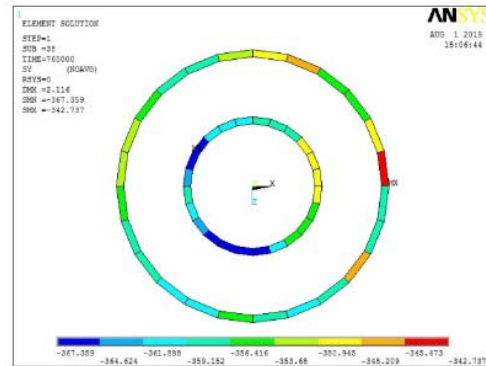


(b) Model No.32

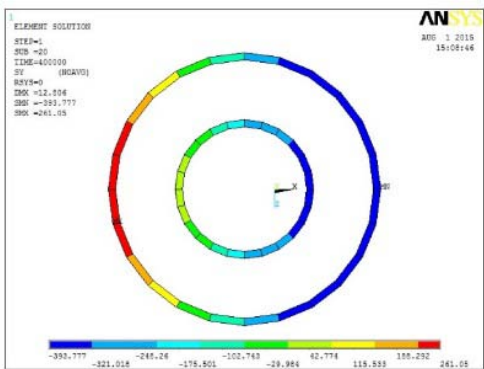
Fig. 19 Stress distribution for the outer and inner steel tubes



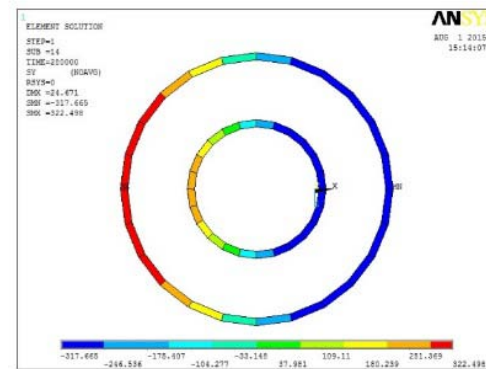
(c) Model No.38



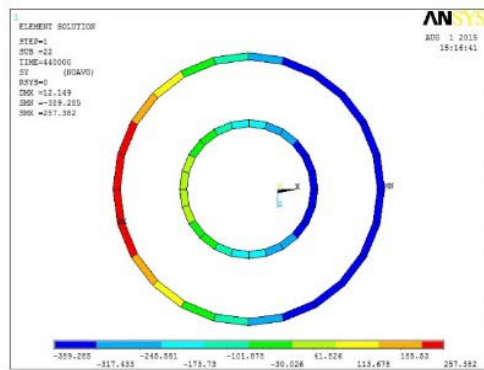
(d) Model No.40



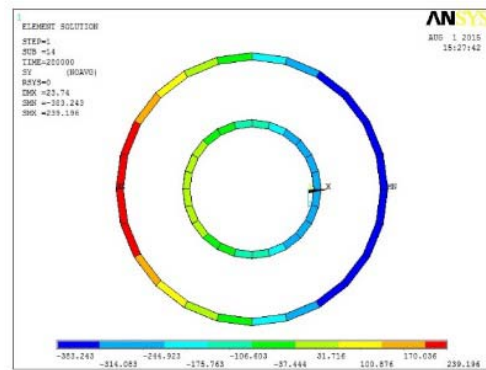
(e) Model No.41



(f) Model No.42



(g) Model No.44



(h) Model No.50

Fig. 19 Continued

3.4 Comparison with available formulas for interaction curves

Interaction equations have been suggested by Han *et al.* (2004) to predict the member capacities of the CFDST beam-columns. Fig. 20 lists a sample comparison between the results of the extensive finite element study and the predictions of the simplified model proposed by Han *et*

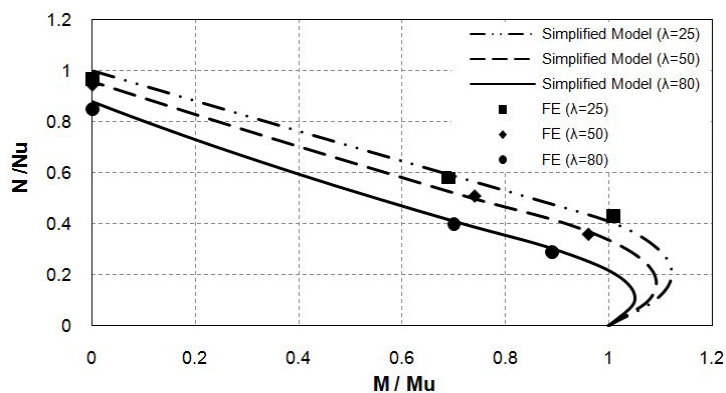


Fig. 20 Interaction curves vs predicted finite element results ($f_y = 235$ MPa, $f_{cu} = 30$ MPa)

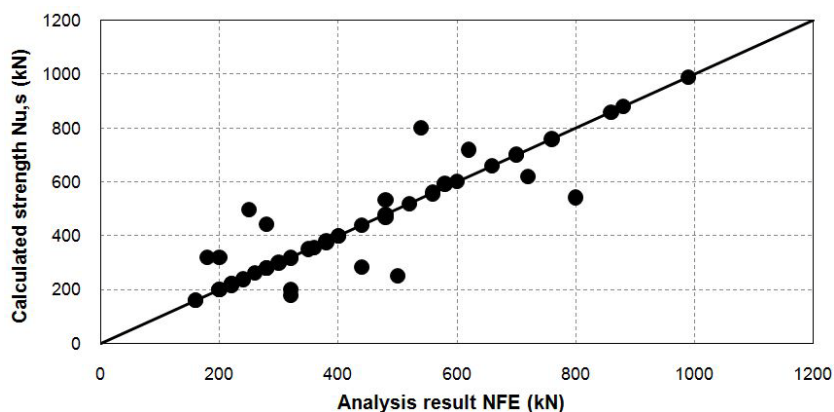


Fig. 21 Comparison of member capacity between the simplified model and the finite element results

al. (2004). As can be seen, the results are in good agreement with the ones predicted by the simplified model. Fig. 21 compares the member capacities as deduced from the finite element models with the ones calculated using the simplified models. A mean of 1.03 along with a coefficient of variation of 0.25 are observed. It is generally observed that the simplified model can predict member capacity for beam-columns with small slenderness ratios. As the value of the slenderness ratio increases, the simplified model underestimates the value of axial member capacity.

4. AISC-360-10 formulas

AISC-360-10 (2010) provides formulas for calculating the ultimate compressive strength of concrete-filled columns. The formulas estimate such value while considering the length effects of columns. Formulas for estimating the capacity of CFDST members are still missing. The approach adopted in AISC-360-10 (2010) is extended in order to calculate the CFDST beam-column capacity. This standard calculates the axial capacity based on the summation of the axial strength

of the different components multiplied by a factor to account for the slenderness of the section. The equations provided by AISC-360-10 (2010) are modified to account for the inner steel tube. The modified equations for the compressive capacity are as follows

$$\text{For } P_{no} / P_e \leq 2.25: \quad P_n = P_{no} \cdot [0.625^{(P_{no} / P_e)}] \quad (3)$$

$$\text{For } P_{no} / P_e > 2.25: \quad P_n = 0.877 \cdot P_e \quad (4)$$

$$P_{no} = f_{yi} \cdot A_{si} + f_{yo} \cdot A_{so} + 0.85 \cdot f_{ck} \cdot A_c$$

$$P_e = \frac{\pi^2 \cdot (EI_{eff})}{(kL)^2}$$

$$EI_{eff} = E_s \cdot (I_{si} + I_{so}) + C_3 \cdot E_c \cdot I_c \quad (5)$$

$$C_3 = 0.6 + 2 \cdot \left[\frac{A_s}{A_s + A_c} \right] \leq 0.9 \quad (6)$$

The flexural capacity is calculated considering the stress distribution cases shown in Fig. 22 while considering that the section is compact and will attain the plastic capacity as the case for the tubes considered in the current study. The force and moment components about the centroid of the cross section depend on the location of the neutral axis and can be calculated considering the equilibrium of the different force components. The normalized interaction equation in AISC-360-10 (2010) for beam-columns is

$$\text{For } \frac{P}{P_n} \geq 0.2: \quad \frac{P}{P_n} + \frac{8}{9} \cdot \frac{M}{M_n} = 1 \quad (7)$$

$$\text{For } \frac{P}{P_n} < 0.2: \quad \frac{P}{2 \cdot P_n} + \frac{M}{M_n} = 1 \quad \frac{P}{2 \cdot P_n} + \frac{M}{M_n} = 1 \quad (8)$$

The capacity of the section is calculated considering the above equations. For simplicity, the nominal flexural capacity of the section is calculated as the plastic section modulus of outer steel tube, inner steel tube, and concrete. Fig. 23 compares the member capacities as deduced from the finite element models with the ones calculated using the modified AISC-360-10 (2010) equations. A mean of 1.97 along with a coefficient of variation of 0.25 are observed. It can be seen that the results are scattered and generally underestimates section capacity. For stub columns, the predictions, provided by the formulas, yield satisfactory values. However, as the length of the column and the compressive strength of concrete increase, the predictions underestimate the capacity by a ratio reaching 2.5. For beam-columns, the predictions underestimate section capacity by an average ratio of 1.5. This can be attributed to the fact that most codes neglect the influence of concrete confinement and concrete tensile strength on section capacity.

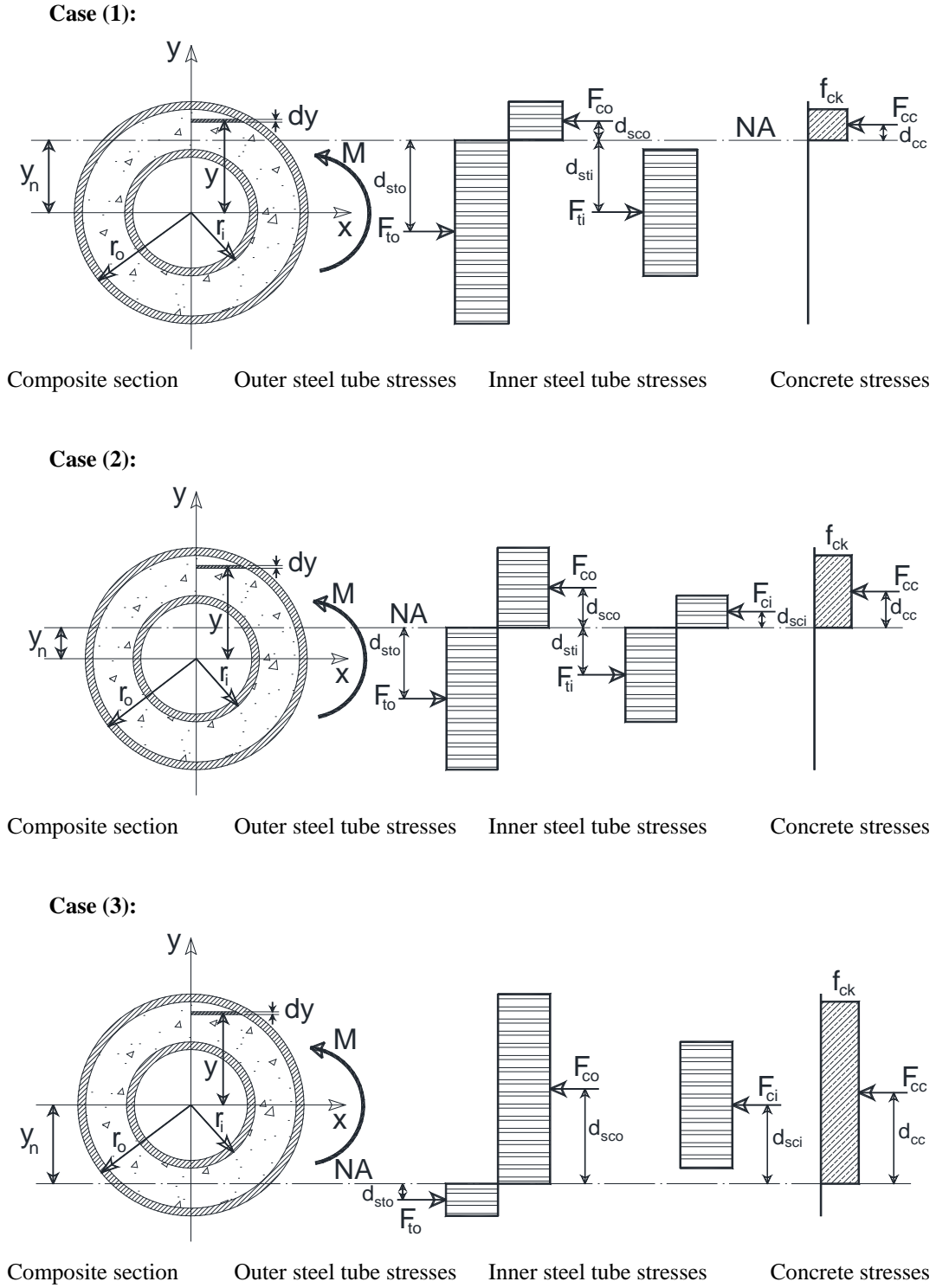


Fig. 22 Ultimate moment capacity of CFDST

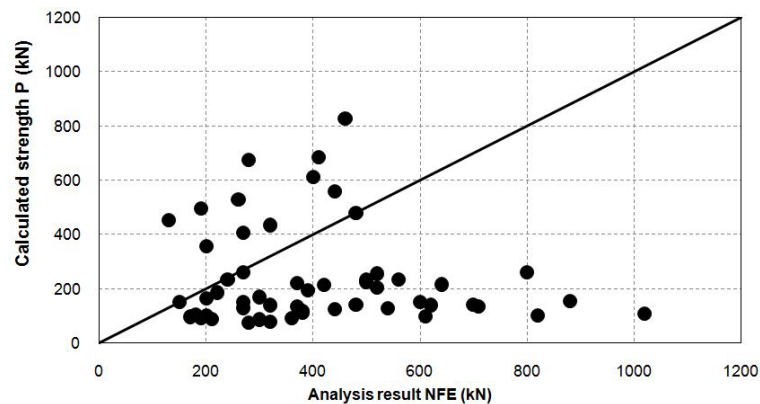


Fig. 23 Comparison of member capacity between the modified AISC-360-10 formula (2010) and the finite element results

5. Conclusions

The ultimate capacity of CFDST beam-columns is investigated through finite element analysis. The accuracy of the models is verified by comparison to past experimental results (Tao *et al.* 2004). Comparison focused on the ultimate axial capacity and the mid-height displacement. Hence, the models are extended and used to perform an extensive parametric study. A total of fifty-four models are built and analyzed using ANSYS software program. The investigated parameters included the load eccentricity, slenderness ratio, and material properties. The ultimate capacity results are deduced from the models and the effect of the different parameters is listed. Comparisons with the formulas provided by previous researchers is presented and evaluated. Predictions by formulas presented by AISC-360-10 (2010) are investigated and assessed. It was found that such formulas underestimate the capacity of the section especially if the section is subjected to combined axial force and flexural bending. Meanwhile, it overestimates the capacity for sections subjected to axial compressive load only.

References

- ACI (2014), Building Code Requirements for Reinforced Concrete; ACI 318-14, American Concrete Institute, Detroit, MI, USA.
- AISC (2010), Specification for Structural Steel Buildings; ANSI/AISC 360, American Institute of Steel Construction, Chicago, IL, 2010.
- Ansys Release 12.0 (YEAR), Theory Reference for Ansys and Ansys Workbench; ANSYS, Inc., Southpointe, 275 Technology Drive, Canonsburg, PA, USA.
- Elchalakani, M., Zhao, X.L. and Grzebieta, R.H. (2002), "Tests on concrete filled double-skin (CHS outer and SHS inner) composite short columns under axial compression", *Thin-Wall. Struct.*, **40**(5), 415-441.
- Han, L.H., Tao, Z., Hong, H. and Zhao, X.L. (2004), "Concrete-filled double skin (SHS outer and CHS inner) steel tubular beam-columns", *Thin-Walled Struct.*, **42**(9), 1329-1355.
- Han, L.H., Huang, H., Tao, Z. and Zhao, X.L. (2006), "Concrete-filled double skin steel tubular (CFDST) beam-columns subjected to cyclic bending", *J. Eng. Struct.*, **28**(12), 1698-1714.
- Han, L.H., Huang, H. and Zhao, X.L. (2009a), "Analytical behaviour of concrete-filled double skin steel tubular (CFDST) beam-columns under cyclic loading", *Thin-Wall. Struct.*, **47**(6-7), 668-680.

- Han, L.H., Li, Y.J., Liao, F.Y. and Tao, Z. (2009b), "Influence of long-term loading on the performance of concrete-filled double skin steel tubular columns: Experiments", *Proceedings of the 6th International Conference on Advances in Steel Structures*, Hong Kong, December.
- Han, L.H., Li, W. and Bjorhovde, R. (2014), "Developments and advanced applications of concrete-filled steel tubular (CFST) structures: Members", *J. Const. Steel Res.*, **100**, 211-228.
- Ho, J.C.M. and Dong, C.X. (2014), "Simplified design model for uni-axially loaded double-skinned concrete-filled-steel-tubular columns with external confinement", *J. Adv. Steel Res.*, **10**(2), 179-199.
- Huang, H., Han, L.H., Zhong, T. and Zhao, X.L. (2010), "Analytical behaviour of concrete-filled double skin steel tubular (CFDST) stub columns", *J. Construct. Steel Res.*, **66**(4), 542-555.
- Lin, M.L. and Tsai, K.C. (2001), "Behavior of double-skinned composite steel tubular columns subjected to combined axial and flexural loads", *Proceedings of the 1st International Conference on Steel and Composite Structures*, Pusan, Korea, June, pp. 1145-1152.
- Lu, H., Zhao, H. and Han, L.H. (2011), "FE modelling and fire resistance design of concrete filled double skin tubular columns", *J. Construct. Steel Res.*, **67**(11), 1733-1748.
- Pagoulatou, M., Sheehan, T., Dai, X.H. and Lam, D. (2014), "Finite element analysis on the capacity of circular concrete-filled double-skin steel tubular (CFDST) stub columns", *J Eng. Struct.*, **72**, 102-112.
- Ren, Q.X., Hou, C., Lam, D. and Han, L.H. (2014), "Experiments on the bearing capacity of tapered concrete filled DOUBLE SKIN STEEL tubular (CFDST) stub columns", *Steel Compos. Struct., Int. J.*, **17**(5), 667-686.
- Tao, Z. and Han, L.H. (2006), "Behaviour of concrete-filled double skin rectangular steel tubular beam-columns", *J. Const. Steel Res.*, **62**(7), 631-646.
- Tao, Z., Han, L.H. and Zhao, X.L. (2004), "Behaviour of concrete-filled double skin (CHS inner and CHS outer) steel tubular stub columns and beam-columns", *J. Constr. Steel Res.*, **60**(8), 1129-1158.
- Zhao, X.L., Grzebieta, R.H. and Elchalakani, M. (2002), "Tests of concrete-filled double skin CHS composite stub columns", *Steel Comp. Struct., Int. J.*, **2**(2), 129-142.
- Uenaka, K. and Kitoh, H. (2009), "Bending-shear behavior of deep concrete filled double steel tubular beam", *Proceedings of the 6th International Conference on Advances in Steel Structures*, Hong Kong, December, pp. 498-505.
- Uenaka, K. and Kitoh, H. (2011), "Mechanical behavior of concrete filled double skin tubular circular deep beams", *Thin-Wall. Struct.*, **49**(2), 256-263
- Uenaka, K., Kitoh, H. and Keiichiro, S. (2008a), "Concrete filled double skin tubular members subjected to bending", *Steel and Compos. Struct., Int. J.*, **8**(4), 297-312.
- Uenaka, K., Shimizu, M. and Kitoh, H. (2008b), "Experimental study on concrete filled double steel tubular beam under bending and shear", *Proceedings of the Japan Concrete Institute*, **30**(3), 1321-1326.
[In Japanese]
- Uenaka, K., Kitoh, H. and Sonoda, K. (2010), "Concrete filled double skin circular stub columns under compression", *Thin-Wall. Struct.*, **48**(1), 19-24.
- Yagishita, F., Kitoh, H., Sugimoto, M., Tanihira, T. and Sonoda, K. (2000), "Double skin composite tubular columns subjected to cyclic horizontal force and constant axial force", *Proceedings of the 6th International Conference on Steel and Concrete Composite Structures*, Los Angeles, CA, USA, March, pp. 497-503.
- Yu, X., Tao, Z., Han, L.H. and Uy, B. (2009), "Residual strength of concrete-filled double-skin steel tubular stub columns after exposure to fire", *Proceedings of the 9th International Conference on Steel Concrete Composite and Hybrid Structures*, Leeds, UK, July, pp. 483-488.